

## GROWTH OF A LOCALIZED SEED MAGNETIC FIELD IN A TURBULENT MEDIUM

JUNGYEON CHO AND HYUNJU YOO

Dept. of Astronomy and Space Science, Chungnam National University, Daejeon, South Korea; jcho@cnu.ac.kr  
*Draft version January 18, 2021*

### ABSTRACT

Turbulence dynamo deals with amplification of a seed magnetic field in a turbulent medium and has been studied mostly for uniform or spatially homogeneous seed magnetic fields. However, some astrophysical processes (e.g. jets from active galaxies, galactic winds, or ram-pressure stripping in galaxy clusters) can provide localized seed magnetic fields. In this paper, we numerically study amplification of localized seed magnetic fields in a turbulent medium. Throughout the paper, we assume that driving scale of turbulence is comparable to the size of the system. Our findings are as follows. First, turbulence can amplify a localized seed magnetic field very efficiently. The growth rate of magnetic energy density is as high as that for a uniform seed magnetic field. This result implies that a magnetic field ejected from an astrophysical object can be a viable source of magnetic field in a cluster. Second, the localized seed magnetic field disperses and fills the whole system very fast. If turbulence in a system (e.g. a galaxy cluster or a filament) is driven at large scales, we expect that it takes a few large-eddy turnover times for magnetic field to fill the whole system. Third, growth and turbulence diffusion of a localized seed magnetic field are also fast in high magnetic Prandtl number turbulence. Fourth, even in decaying turbulence, a localized seed magnetic field can ultimately fill the whole system. Although the dispersal rate of magnetic field is not fast in purely decaying turbulence, it can be enhanced by an additional forcing.

*Subject headings:* ISM:general - intergalactic medium - MHD - turbulence

### 1. INTRODUCTION

The origin and growth of magnetic field in the universe is an important unsolved problem in astrophysics (Kulsrud & Zweibel 2008). Earlier studies have shown that turbulence can efficiently amplify a weak seed magnetic field. The main mechanism that is responsible for the amplification is stretching of magnetic field lines (Batchelor 1950; Zel'dovich et al. 1984; Childress & Gilbert 1995). This process is called *turbulence dynamo* (or *small-scale dynamo*) and should not be confused with *mean field dynamo* (or *large-scale dynamo*), which deals with generation/growth of a large-scale magnetic field.

Small-scale turbulence dynamo has been studied since 1950s (see, e.g., Batchelor 1950; Kazantsev 1968; Kulsrud & Anderson 1992; Kulsrud et al. 1997; Cho & Vishniac 2000; Schekochihin et al. 2004; Brandenburg & Subramanian 2005; Schekochihin & Cowley 2007; Ryu et al. 2008; Cho et al. 2009). When we introduce a weak *uniform* magnetic field in a turbulent medium, amplification of the uniform field happens in three stages (see Schekochihin & Cowley 2007; see also Cho & Vishniac 2000, Cho et al. 2009). (1) Stretching of magnetic field lines occurs most actively near the velocity dissipation scale first, and the magnetic energy grows exponentially. Note that eddy motions in turbulence are fastest at the velocity dissipation scale. (2) The exponential growth stage ends when the magnetic energy becomes comparable to the kinetic energy at the dissipation scale. The subsequent stage is characterized by a linear growth of magnetic energy and a gradual shift of the peak of magnetic field spectrum to larger scales. (3) The amplification of magnetic field stops when the magnetic energy density becomes comparable to the kinetic energy density and a final, statistically steady, saturation stage begins.

Knowledge on turbulence dynamo is useful for understanding the origin of magnetic fields in many astrophysical fluids. For example, Ryu et al. (2008) numerically studied amplification of the intergalactic magnetic field by the dynamo action of turbulence. They assumed that turbulence is generated by cosmological shocks, which are produced when primordial gases fall into the gravitational potential well caused by dark matters in clusters and filaments (Ryu et al. 2003). For simplicity, they assumed that a weak uniform seed magnetic field fills the whole system at the beginning of the simulation. They found that turbulence is strong in the intracluster medium (ICM) and, therefore, has almost reached the saturation stage and that turbulence in filaments is weak and in early linear stage. Based on a more quantitative analysis, they estimated that the average magnetic field strength would be a few  $\mu\text{G}$  inside clusters/groups, approximately  $0.1 \mu\text{G}$  around clusters/groups, and approximately  $10 \text{ nG}$  in filaments.

Existence of regular magnetic fields in many astrophysical fluids, such as the interstellar medium (ISM), justifies the use of uniform seed magnetic fields in turbulence dynamo studies. However, there are astrophysical systems where existence of regular fields is uncertain. For example, it is not clear whether or not regular fields exist in the ICM. If seed magnetic fields are relic primordial fields (Rees 1987; Kronberg 1994; Dolag, Bartelmann & Lesch 1999, 2002; Gnedin, Ferrara & Zweibel 2000; Banerjee & Jedamzik 2003; Murgia et al. 2004; Brügggen et al. 2005; Dubois & Teyssier 2008), the correlation length of the seed fields can be very large and we may have regular fields in the ICM. On the other hand, if seed magnetic fields have astrophysical origins (e.g. jets from active galaxies, galaxy winds, and ram-pressure stripping, etc.; see Rephaeli 1988 for an ear-

lier discussion on the origin of the ICM magnetic fields through ram-pressure stripping), we will probably have no regular fields in the ICM. In the latter case, we expect that seed magnetic fields ejected from astrophysical objects are highly localized in space. Then a question arises: how do these localized seed magnetic fields grow? In this paper, we study amplification of localized seed magnetic fields in a turbulent medium.

Earlier cosmological simulations have shown that magnetic fields ejected from active galactic nuclei (AGNs) (Ensslin et al. 1997; Völk & Atoyan 2000; Donnert et al 2009; Xu et al. 2010, 2011) or normal galaxies through galactic winds (Kronberg, Lesch & Hopp 1999; Bertone, Vogt & Ensslin 2006) or ram-pressure stripping (Arieli, Rephaeli & Norman 2011) can be dispersed and amplified by turbulence and are viable origins of magnetic fields in galaxy clusters. Xu et al. (2010), for example, showed that “as long as the AGN magnetic fields are ejected before the major mergers in the cluster formation history, magnetic fields can be transported throughout the cluster and can be further amplified by the ICM turbulence caused by hierarchical mergers during the cluster formation process.” However, those simulations are compressible ones and it is usually difficult to obtain converging results free from numerical effects in compressible turbulence simulations (see discussions in Ryu et al. 2008). Therefore it is advantageous to use an incompressible code because we can control numerical viscosity and resistivity in incompressible codes.

In this paper, we use an incompressible code with hyper-viscosity and hyper-diffusion, so that we have virtually zero intrinsic numerical viscosity and diffusion, and the maximized inertial range. We assume that driving scale of turbulence is comparable to the size of the whole system, which would be true if turbulence is produced by cosmological shocks or major mergers in galaxy clusters. We also assume that the seed magnetic field has a doughnut shape at  $t=0$ . We describe numerical method in Section 2, and we present results in Section 3. We give discussions in Section 4 and the summary in Section 5.

## 2. NUMERICAL METHODS

We use a pseudospectral code to solve the incompressible MHD equations in a periodic box of size  $2\pi$ :

$$\frac{\partial \mathbf{v}}{\partial t} = -(\nabla \times \mathbf{v}) \times \mathbf{v} + (\nabla \times \mathbf{B}) \times \mathbf{B} + \nu \nabla^2 \mathbf{v} + \mathbf{f} + \nabla P', \quad (1)$$

$$\frac{\partial \mathbf{B}}{\partial t} = \nabla \times (\mathbf{v} \times \mathbf{B}) + \eta \nabla^2 \mathbf{B}, \quad (2)$$

$$\nabla \cdot \mathbf{v} = \nabla \cdot \mathbf{B} = 0, \quad (3)$$

where  $\mathbf{f}$  is random driving force,  $P' \equiv P + \mathbf{v} \cdot \mathbf{v}/2$ ,  $\mathbf{v}$  is the velocity, and  $\mathbf{B}$  is magnetic field divided by  $(4\pi\rho)^{1/2}$ . We use 22 forcing components with  $2 \leq k \leq \sqrt{12}$ . Each forcing component has correlation time of  $\sim 1$ . The peak of energy injection occurs at  $k \approx 2.5$ . In our simulations with  $\nu = \eta$ ,  $v \sim 1$  during the growth stage and  $\sim 0.8$  during the saturation stage (see Figure 1). Therefore, one eddy turnover time at the outer scale of turbulence (or large-eddy turnover time),  $\sim L/v$ , is approximately  $\sim 2.5$  and  $\sim 3$  time units, respectively. Since  $v \sim 1$ ,  $\mathbf{v}$  can be viewed as roughly the velocity measured in units of the r.m.s. velocity of the system and  $\mathbf{B}$  as the Alfvén

speed in the same units. Other variables have their usual meaning.

In pseudospectral methods, we calculate the temporal evolution of the equations (1) and (2) in Fourier space. To obtain the Fourier components of nonlinear terms, we first calculate them in real space, and transform back into Fourier space. We use exactly same forcing terms for all simulations. We use an appropriate projection operator to calculate  $\nabla P'$  term in Fourier space and also to enforce divergence-free condition ( $\nabla \cdot \mathbf{v} = \nabla \cdot \mathbf{B} = 0$ ). We use up to  $512^3$  collocation points.

At  $t = 0$ , the magnetic field has a doughnut shape, which mimics a magnetic field ejected by a galactic outflow<sup>1</sup>. We use the following expression for the magnetic field at  $t=0$ :

$$\mathbf{B}(r_\perp, \Delta x) = \frac{B_{max}}{2\sigma_0^2 e^{-1}} r_\perp^2 e^{-r_\perp^2/2\sigma_0^2} e^{-\Delta x^2/8\sigma_0^2} \hat{\theta}_\perp, \quad (4)$$

where  $\sigma_0 = 4\sqrt{2}$ ,  $r_\perp = (\Delta y^2 + \Delta z^2)^{1/2}$ , and  $\Delta x, \Delta y$ , and  $\Delta z$  are distances measured from the center of the numerical box in grid units. The unit vector  $\hat{\theta}_\perp$  is perpendicular to  $(\Delta x, 0, 0)$  and  $(0, \Delta y, \Delta z)$ . Note that the maximum strength of the magnetic field at  $t=0$  is  $B_{max}$ . Since  $\sigma_0 = 4\sqrt{2}$  in Equation (4), the size of the magnetized region at  $t=0$  is  $\sim 16$  in grid units, which is  $\sim 1/16$  of the whole system for runs with  $256^3$  grid points and  $\sim 1/32$  for  $512^3$ . Therefore, in a cluster of size  $\sim 1Mpc$ , the size of the initially magnetized region corresponds to  $\sim 60kpc$  and  $\sim 30kpc$ , respectively.

Hyperviscosity and hyperdiffusion are used for dissipation terms. The power of hyperviscosity is set to 3, such that the dissipation term in the above equation is replaced with

$$- \nu_n (\nabla^2)^n \mathbf{v}, \quad (5)$$

where  $n = 3$ . The same expression is used for the magnetic dissipation term. We list parameters used for the simulations in Table 1. Diagnostics of our code can be found in Cho & Vishniac (2000).

## 3. RESULTS

### 3.1. Turbulence with unit magnetic Prandtl number ( $\nu = \eta$ )

Figure 1 shows time evolution of  $v^2$  and  $B^2$  for different values of  $B_{max}$ . The initial magnetic field has a doughnut shape (see Equation [4]) and  $B_{max}$  is the maximum strength of the initial magnetic field. As in the uniform seed magnetic field cases, growth of magnetic energy density occurs in three stages. Magnetic energy grows exponentially first. We can see the exponential growth in the lower panel of Figure 1, where we use a logarithmic scale for the y-axis. When  $B_{max}$  is small (see, for example,  $256-B_{max}0.001$  and  $256-B_{max}0.01$ ), the growth rate is virtually independent of the value of  $B_{max}$ . Then a slower linear growth stage follows, which we can clearly observe in the upper panel of the figure. All runs show similar growth rates in this stage. Finally, after  $t \sim 20$  in units of  $L/v$  ( $\sim 2.5$  in code time units), a statistically

<sup>1</sup> Note however that we use a weak uniform seed magnetic field for the reference runs REF256 and REF256-Pr, in which the strength of the mean field,  $B_0$ , is 0.0001 and we have only the mean field at  $t=0$ .

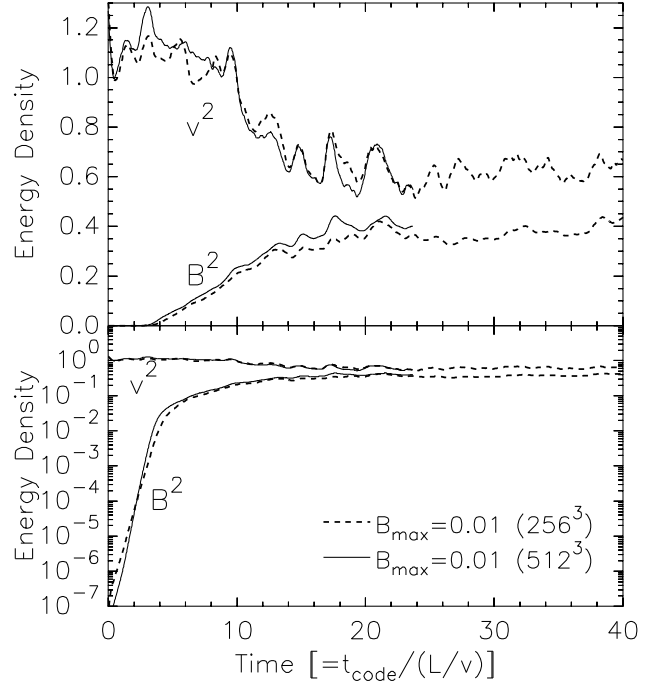
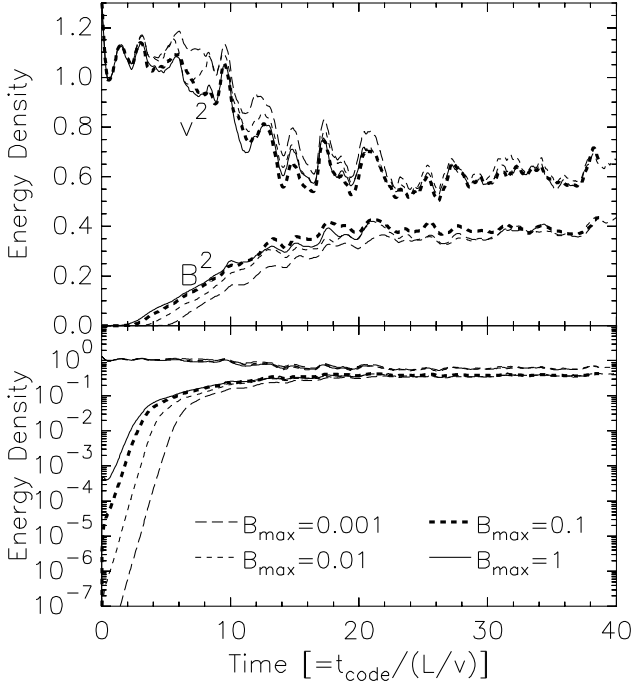


FIG. 1.— Time evolution of  $B^2$  and  $v^2$  in runs with  $\nu = \eta$ . Each run starts from a fully developed turbulent velocity field and a localized seed magnetic field. The localized seed magnetic fields have a doughnut shape. All runs have the same numerical resolution. Different lines denote different values of  $B_{max}$ . Time is given in units of the large-eddy turnover time defined by  $L/v$ :  $t \equiv t_{code}/(L/v)$ , where  $t_{code}$  is time in code units,  $L$  ( $\sim 2.5$ ) is the outer-scale of turbulence and  $v$  ( $\sim 1$ ) is the r.m.s. velocity *before* the saturation stage. Results are from  $256-B_{max}0.001$ ,  $256-B_{max}0.01$ ,  $256-B_{max}0.1$ , and  $256-B_{max}1$ . Note the logarithmic scale for the vertical axis in the lower panel.

FIG. 2.— Resolution study. We compare results of  $256-B_{max}0.01$  and  $512-B_{max}0.01$ . Two runs have different numerical resolutions, but other numerical setups are the same. Two results show good agreements. Note the logarithmic scale for the vertical axis in the lower panel.

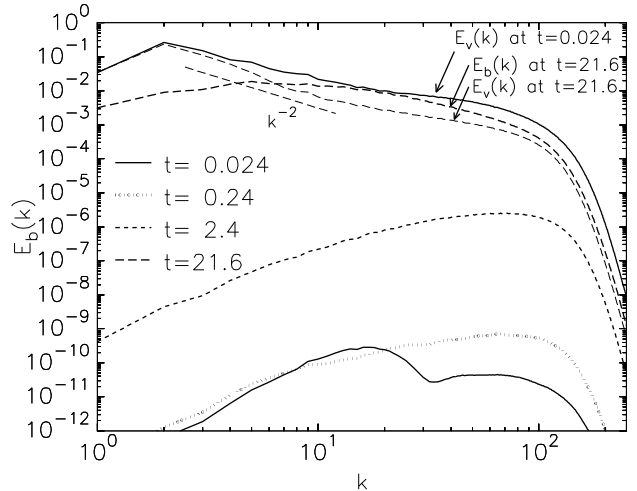
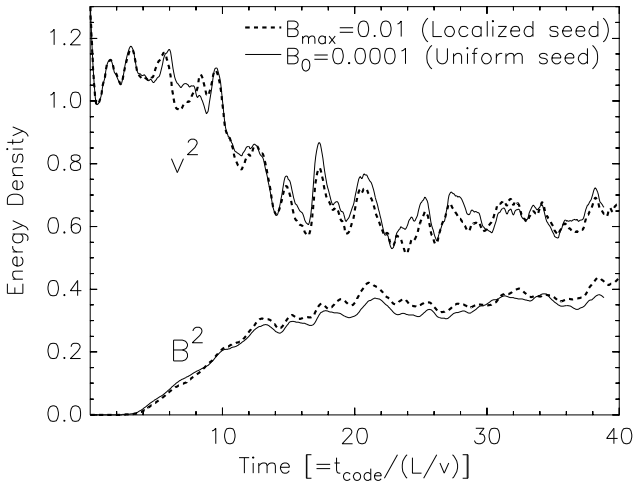


FIG. 3.— Comparison with the case of a uniform seed magnetic field. We compare the results of  $256-B_{max}0.01$  and REF256. Note that we use a localized seed magnetic field in the former and a uniform seed field ( $B_0 = 0.0001$ ) in the latter. We find a good correspondence between two results.

FIG. 4.— Time evolution of magnetic spectrum. The initial seed magnetic field (see the solid curve) loses its original shape quickly and forms a spectrum that has a peak near the dissipation scale (see the dotted curve). Then the spectrum goes up without changing the shape much (see the dashed line). At this point, the seed magnetic field already fills the most of the simulation box (see Figure 5 and Figure 6). After magnetic field fills the whole volume, time evolution of magnetic spectrum and energy density should be very similar to those of weak uniform seed magnetic field cases. Time is given in units of  $L/v$ . From Run  $512-B_{max}0.01$ .

stationary saturation stage is reached. The saturation level of magnetic energy density is comparable to the kinetic energy density. Figure 1 shows that the stronger the seed magnetic field (or  $B_{max}$ ) is, the earlier the linear growth stage begins and the sooner the saturation stage is reached.

Resolution study shows that the linear growth rate does not strongly depend on the numerical resolution. In Figure 2, we compare Runs 512- $B_{max}0.01$  and 256- $B_{max}0.01$ , in which the shape of seed magnetic field (see Equation [4]) and numerical setup are identical and only the numerical resolutions are different. As we can see in the figure, the overall results are very similar. That is, the growth rates at the linear growth stage and the saturation levels of the magnetic energy density are very similar. In the lower panel of the figure, we plot the same quantities, but we use a logarithmic scale for the y-axis. The lower panel shows the growth rate of Run 512- $B_{max}0.01$  during the exponential growth stage is higher than that of 256- $B_{max}0.01$ , which is due to the fact that the eddy turnover time at the velocity dissipation scale of Run 512- $B_{max}0.01$  is shorter.

According to Figure 1, the growth rate of magnetic energy during the linear growth stage seems to be independent of the value of  $B_{max}$ . The linear growth rate in Figure 1 is also in good correspondence with that of uniform seed magnetic field cases. When we compare the linear growth rates of Run 256- $B_{max}0.01$  (localized seed magnetic field) and Run REF256 (uniform seed magnetic field), they are very similar (Figure 3). The saturation levels of the magnetic energy density in both simulations are also very similar.

Three stages of magnetic energy growth are also supported by the time evolution of magnetic spectrum. Figure 4 shows how magnetic spectrum  $E_b(k)$  of Run 512- $B_{max}0.01$  evolves with time. When  $t \lesssim 10$ , stretching happens near the dissipation scale and, therefore, magnetic energy spectrum peaks there. As magnetic field is amplified by stretching, the magnetic spectrum moves upward without changing its shape much (compare, for example, spectra for  $t=0.24$  and  $t=2.4$ ). When magnetic spectrum ‘touches’ the velocity spectrum  $E_v(k)$  at the dissipation scale, the exponential growth ends and the slower linear growth stage follows. Note that, when magnetic spectrum ‘touches’ the velocity spectrum at the dissipation scale, the magnetic energy density is approximately  $\sim (k_d/k_L)^{2/3}$  times the kinetic one, where  $k_d$  is the dissipation scale wavenumber and  $k_L \sim 2.5$ , and it becomes ‘visible’ in Figure 2. The long dashed curves are the spectra of velocity and magnetic field during the saturation stage. Velocity spectrum  $E_v(k)$  peaks at the energy injection scale and magnetic spectrum  $E_b(k)$  peaks at a smaller scale. The logarithmic slope of the velocity spectrum during the saturation stage is steeper than  $-5/3$  for  $k \lesssim 10$  and gets shallower for  $k \gtrsim 10$ . The behavior of magnetic energy spectrum is very similar to that of a uniform seed field case (see, for example, Cho et al. 2009).

So far, we have found surprising similarities between localized and uniform seed magnetic fields. They both follow similar growth stages, show similar growth rates at the linear growth stage, reach similar levels of magnetic energy saturation, and exhibit similar time evolution of

magnetic spectrum. Then why are they all similar? The answer is fast magnetic diffusion. Turbulence enhances diffusion processes. Figure 5 visualizes fast magnetic diffusion in Run 256- $B_{max}0.01$ . The localized initial magnetic field (left panel) spreads out by turbulent motions. Note that it takes only  $\sim 2.4$  large-eddy turnover times for the localized initial magnetic field to fill virtually the whole box (see the right panel). The large-eddy turnover time is defined as  $L/v$ , where  $L$  ( $\sim 2.5$ ) is the outer scale and  $v$  ( $\sim 1$ ) the r.m.s. velocity. Therefore, turbulence makes the localized seed magnetic field fill the whole system within less than  $\sim 3$  large-eddy turnover times. After magnetic field fills the whole box, time evolution of magnetic energy density should be very similar to that of uniform or spatially homogeneous magnetic field cases (see, for example, Cho et al. 2009).

Figure 6 confirms fast diffusion of magnetic field, in which we plot the standard deviation,  $\sigma$ , of magnetic field distribution:

$$\sigma = (\sigma_x^2 + \sigma_y^2 + \sigma_z^2)^{1/2}, \quad (6)$$

$$\sigma_i^2 = \frac{\int (x_i - \bar{x}_i)^2 |\mathbf{B}(\mathbf{x}, t)|^2 d^3x}{\int |\mathbf{B}(\mathbf{x}, t)|^2 d^3x}, \quad (7)$$

$$\bar{x}_i = \frac{\int x_i |\mathbf{B}(\mathbf{x}, t)|^2 d^3x}{\int |\mathbf{B}(\mathbf{x}, t)|^2 d^3x}, \quad (8)$$

where  $i = x, y, \text{ and } z$  and  $\sigma$  shown in the plot is normalized by the box size. Initially the standard deviation rises very quickly, which is due to diffusion of magnetic field within an energy-containing eddy. The duration of the quick rise is about 1.5 large-eddy turnover times, if we define the large-eddy turnover time as  $L/v$ . The slower growth after  $t/(L/v) \sim 1.5$  is due to a slower diffusion of magnetic field on scales larger than the outer scale of turbulence. The behavior of  $\sigma$  is not sensitive to the value of  $B_{max}$ .

Richardson’s law states that the mean square separation of two passive particles,  $\sigma_m$ , satisfies

$$\frac{d\sigma_m}{dt} \sim \epsilon^{1/3} \sigma_m^{1/3}. \quad (9)$$

Therefore, we may write

$$\sigma(t)^{2/3} - \sigma(t_0)^{2/3} \propto t - t_0. \quad (10)$$

(see, for example, Lesieur 1990; see also Cho et al. 2003). The inset shows  $\sigma^{2/3}$  of magnetic field distribution roughly follows the Richardson’s law when  $t/(L/v) \lesssim 1.5$ .

### 3.2. Turbulence with a high magnetic Prandtl number ( $\nu \gg \eta$ )

The viscosity in galaxy clusters may not be negligible (Schekochihin et al. 2004; Ruszkowski et al. 2004; Reynolds et al. 2005; Subramanian, Shukurov & Haugen 2006), while the magnetic diffusivity is still very small. In fact, if we use the Spitzer (1962) formula for the viscosity, the Reynolds number  $Lv/\nu$ , where  $L$  is the outer scale of turbulence in a cluster,  $v$  the r.m.s. velocity, and  $\nu$  the viscosity, is less than  $\sim 10^3$ . Therefore, the magnetic Prandtl number ( $\nu/\eta$ ) may be very large in the ICM. In this subsection, we consider growth of localized seed magnetic fields in turbulence with non-negligible viscosity. The Reynolds number ( $Lv/\nu$ ) we use in this section

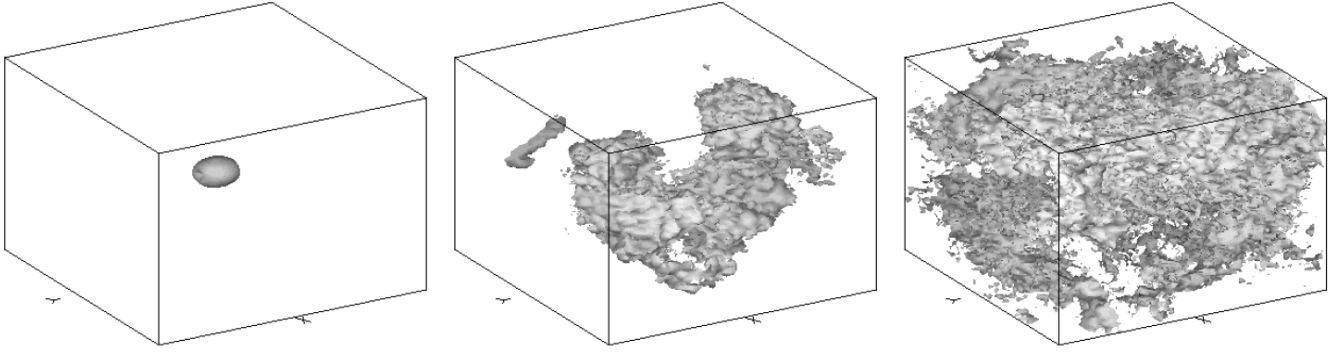


FIG. 5.— Turbulence diffusion of magnetic field. From left to right panels, snapshots at  $t=0$ , 1.2, and 2.4 are shown. The seed magnetic field has a doughnut shape at  $t=0$ . At  $t=2.4$ , the localized seed field fills the most of the computational box. Here time ( $t$ ) is measured in units of  $L/v$ . From 256- $B_{max}0.01$ .

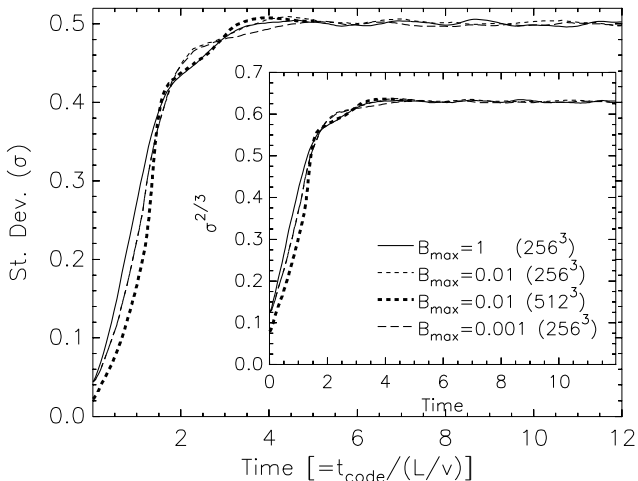


FIG. 6.— Time evolution of the standard deviation of magnetic field distribution. The standard deviation is normalized by the box size, so that it becomes 0.5 when a homogeneous magnetic field fills the whole box. The standard deviation rises quickly when  $t \lesssim 1.5$  large-eddy turnover times, which happens when the localized magnetic field fills the whole energy-containing eddy. After  $t \sim 1.4$  large-eddy turnover times, the diffusion rate of the magnetic field slows down. It takes  $\sim 3$  large-eddy turnover times for the magnetic field to fill the whole box. Results are from 256- $B_{max}0.001$ , 256- $B_{max}0.01$ , 256- $B_{max}1$ , and 512- $B_{max}0.01$ .

is  $\sim 100$ . The magnetic diffusivity is negligibly small because we use a hyper-diffusion.

Figure 7(a) shows time evolution of  $B^2$  and  $v^2$ . Due to non-negligible viscosity in those simulations, small-scale velocity is strongly damped and the inertial range of turbulence is poorly resolved. Indeed the velocity spectrum at  $t=0.0693$  (solid curve) in Figure 7(b) confirms this. Therefore, stretching of magnetic field lines happens at a scale very close to the outer scale of turbulence and the growth rate of magnetic energy density is mostly exponential (see Figure 7(c); see also next paragraph for further discussions). Figure 7(a) shows that it takes less than  $\sim 15$  large-eddy turnover times for the runs to reach the saturation stage. Comparing with Figure 1, we note that growth of magnetic field is at least as fast as that of unit magnetic Prandtl number cases. Note that the large-eddy turnover time  $L/v$  in high magnetic Prandtl

number cases is approximately 2.6 in code units before saturation and 4.5 in code units after saturation.

It seems that growth of a localized seed magnetic field also happens in 3 stages in a high magnetic Prandtl number turbulence<sup>2</sup>.

1. First, we can clearly observe the exponential growth stage in Figure 7(c). The exponential growth stage ends when the magnetic energy density becomes comparable to the kinetic energy density at the stretching scale. Since the stretching scale is very close to the outer scale of turbulence in our simulations, the exponential stage ends when magnetic energy density becomes comparable to the *total* kinetic energy density. Therefore, the exponential stage takes most of the growth time in the high magnetic Prandtl number turbulence. Velocity spectrum does not change much during the exponential stage (compare  $E_v(k)$ 's at  $t=0.693$  and 8.54 in Figure 7(b)), which means that magnetic back-reaction is negligible during the exponential growth stage.
2. Second, after the exponential growth stage, a slower growth stage follows. In Run 512- $B_{max}0.01$ -Pr, the slower growth stage is relatively short due to proximity between the outer scale and the initial stretching scale: it begins at  $t \sim 12$  and ends at  $t \sim 17$ . According to Figure 7(a), the growth rate during the slower growth stage is roughly linear. The growth rate of  $B^2$  during the slower growth stage can be estimated as follows. If stretching happens at a scale  $l$ , we can write

$$\frac{dB^2}{dt} \propto \frac{B^2}{l/v_l} = \frac{B^2 v_l}{l} \quad (11)$$

(see Schekochihin & Cowley 2007), where  $v_l$  is the r.m.s. velocity at the scale  $l$ . The stretching scale  $l$  increases during the slower growth stage. The peak of the magnetic spectrum in Figure 7(b) moves to smaller wavenumbers (compare magnetic spectra at  $t=12.69$ , 13.62, and 20.08), which might indi-

<sup>2</sup> For a related discussion on the case of a weak uniform seed magnetic field, see, for example, Schekochihin & Cowley (2007).

cate increase of the stretching scale. The velocity spectrum between  $k \sim 3$  and  $k \sim 10$  becomes quickly suppressed as soon as the slower growth stage begins (compare velocity spectra at  $t=12.69$  and  $t=13.62$ ). The wavenumbers at which velocity spectrum is suppressed might have something to do with the stretching scale during the exponential growth stage. After the suppression, the stretching scale is clearly the outer scale of turbulence (see the shape of  $E_v(k)$ 's at  $t=13.62$  and  $20.08$ ). Therefore, the behavior of velocity spectrum also suggests increase of  $l$ . We also note that decrease of  $v$  is not negligible during the slower growth stage:  $v^2$  drops fast after  $t \sim 12$  in Run 512- $B_{max}0.01$ -Pr. All in all, increase of  $B^2$ , decrease  $v$  ( $\sim v_l$ ), and increase of  $l$  make the right-hand side of Equation (11) roughly constant, which results in a roughly linear growth rate of  $B^2$  in our simulations.

3. Third, after the slower growth stage, the saturation stage begins. In Run 512- $B_{max}0.01$ -Pr, it begins at  $t \sim 17$ .

During the exponential growth stage, we can write  $B^2 \sim B^2(t=0)\exp(t/\tau)$ , where  $\tau$  is approximately a constant times the large-eddy turnover time<sup>3</sup>. Therefore, the growth time of magnetic field depends on the value of  $B_{max}$ . Indeed, the figure shows that the run with  $B_{max} = 1$  reaches the saturation stage more quickly than smaller  $B_{max}$  cases. Run 512- $B_{max}0.01$ -Pr (thick dashed curves) reaches the saturation stage later than Run 256- $B_{max}0.01$ -Pr (thin dashed curves), because the size of the initially magnetized region normalized by the system size is smaller in the former, which makes  $B^2(t=0)$  smaller in the former. If the seed magnetic field is extremely weak, it is possible that the growth of magnetic field is slower in high magnetic Prandtl number turbulence than in the unit Prandtl number cases with the same seed magnetic field.

As in the unit Prandtl number cases, the seed magnetic fields fills the computational box very fast. According to Figure 7(d), it takes less than  $\sim 4$  large-eddy turnover times for the seed fields to fill the whole box. Roughly speaking, the standard deviation of magnetic field distribution,  $\sigma$ , grows exponentially when  $B_{max}$  is weak. Consider a magnetized region of size  $\sigma$  with  $\sigma < L$ . Then, since stretching happens near the outer-scale of turbulence, the timescale for a substantial change of  $\sigma$  is roughly the large-eddy turnover time  $L/v$ . Therefore, we have the relation

$$\frac{\Delta\sigma}{\Delta t} \propto \frac{\sigma}{L/v} \propto \sigma, \quad (12)$$

which implies exponential growth of  $\sigma$  when  $\sigma < L$ . The inset of Figure 7(d), in which the vertical axis is drawn in logarithmic scale, supports exponential growth of  $\sigma$ .

### 3.3. Decaying turbulence

If the ICM turbulence is driven by temporarily intermittent events, such as mergers, the ICM will undergo disruption and relaxation repeatedly. In this subsection,

<sup>3</sup> In our simulations,  $\tau$  might be the eddy turnover time at  $k \sim 10$  (see the previous footnote)

we study growth of a localized seed magnetic field in turbulence with episodic driving.

To see if a single merger can disperse a localized seed magnetic field, we first perform a decaying turbulence simulation (Run 256- $B_{max}0.01$ -f0). At  $t=0$ , we have a fully developed turbulence and a localized seed magnetic field with  $B_{max}=0.01$ . The shape of the seed magnetic field is given in Equation (4). Then we let the turbulence decay without forcing it. The solid curve in the left panel of Figure 8 shows that the standard deviation  $\sigma$  of the magnetic field distribution gradually rises and converges to the value of 0.5 within  $\sim 10$  initial large-eddy turnover times ( $L/v_{t=0}$ ). Therefore, we can conclude that even a decaying turbulence can make a localized seed field fill the whole system if the driving scale of turbulence is comparable to the system size. The inset in Figure 8 shows that  $v^2$  immediately decreases as turbulence decays, while  $B^2$  rises for  $\sim 10$  large-eddy turnover times and then levels off. As a result, the ratio of magnetic to kinetic energy densities increases.

The results of decaying turbulence simulation imply that a single merger (with magnetic field injection at the end of the merger) would be enough to magnetize the whole ICM. Consider a localized seed magnetic field in a cluster with driving scale of  $\sim 400$  kpc and initial velocity dispersion of  $\sim 400$  km/sec. Then the large-eddy turnover time is  $\sim 10^9$  years. Our result in Figure 8 suggests that the decaying turbulence can magnetize surrounding  $\sim 1$  Mpc region of the cluster within the age of the universe.

Of course, a faster magnetization is possible when we apply additional forcing. For example, we may allow for short-lasting driving after we inject a localized seed magnetic field, which mimics a seed magnetic field injection during a merger. We perform a simulation to see the effect of additional forcing (Run 256- $B_{max}0.01$ -f3). The numerical setups are identical to those of the decaying turbulence simulation. However, in this case we drive turbulence for 3 code time units, which is slightly larger than one large-eddy turnover time  $L/v \sim 2.5$  code time units. After  $t = 3$  code time units, we turn off forcing and let the turbulence decay. We plot the result in the left panel of Figure 8 (see the dashed curve), where we can see that  $\sigma$  rises to a value very close to the saturation value of 0.5 within a couple of large-eddy turnover times. Note that the strength of turbulence is not a crucial factor here. Whatever the strength of the turbulence is, a decaying turbulence can virtually seed the whole system within a couple of large-eddy turnover times. But, if the strength of turbulence is very weak, the large-eddy turnover time can be very long. The inset shows that magnetic energy density rises for  $\sim 10$  code time units and then levels off, while kinetic energy density begins to decrease right after we turn off forcing at  $t = 3$  (in code units). The magnetic energy density in this simulation (dashed curve) is slightly higher than that of purely decaying turbulence (solid curve). From this simulation and the purely decaying turbulence simulation, we can conclude that even a single merger is marginally enough to seed the whole cluster. However, the resulting magnetic field in this case may not be so strong (see values of  $B^2$  in the inset).

The right panel of Figure 8 shows time evolution of

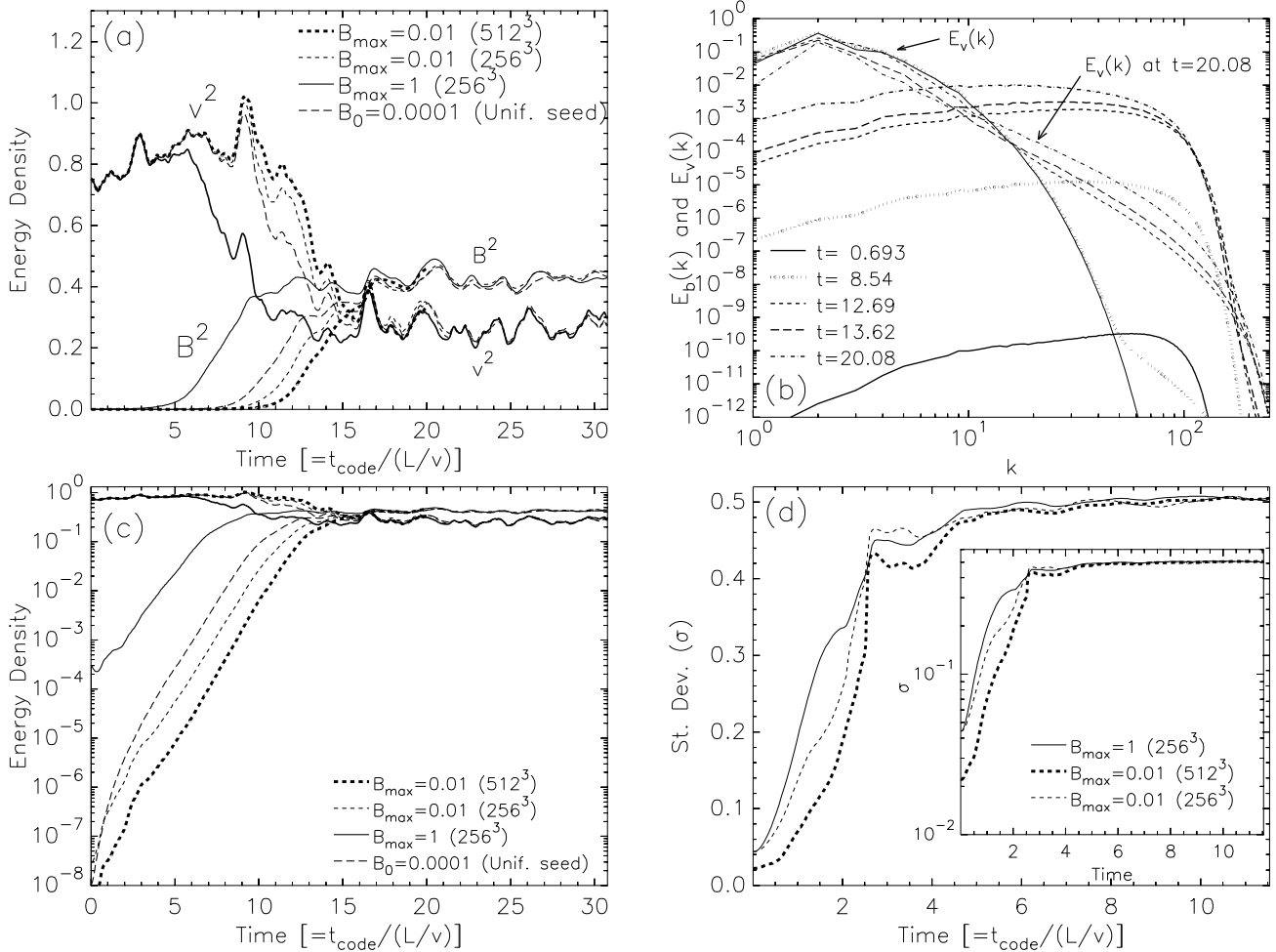


FIG. 7.— High magnetic Prandtl number turbulence ( $\nu \gg \eta$ ). (a) Time evolution of  $B^2$  and  $v^2$ . In all simulations, the Reynolds number is  $\sim 100$  and the magnetic Reynolds number is very large because we use a hyper-diffusivity. Except in case of  $B_0 = 0.0001$ , where we use a uniform seed magnetic field, we use a localized seed magnetic field. Time is given in units of the large-eddy turnover time defined by  $L/v$ , where  $L$  ( $\sim 2.5$ ) is the outer-scale of turbulence and  $v$  ( $\sim \sqrt{0.9}$ ) is the r.m.s. velocity *before* the saturation stage. We observe fast growth of magnetic field. Results are from Runs 512- $B_{\max}0.01$ -Pr, 256- $B_{\max}0.01$ -Pr, 256- $B_{\max}1$ -Pr, and REF256-Pr. (b) Time evolution of velocity and magnetic spectra. Note that the velocity spectrum does not change much during the exponential growth stage. From Run 512- $B_{\max}0.01$ -Pr. (c) Same as (a), but the vertical axis is drawn on logarithmic scale. Note that all simulations with weak  $B_{\max}$  have similar growth rates during the exponential stage. This is because the stretching scales are virtually same in the simulations. In Run 512- $B_{\max}0.01$ -Pr, the exponential growth stage ends at  $t \sim 12$ . (d) Standard deviation of magnetic field distribution. The localized seed magnetic field fills the whole box within  $\sim 3$  to 4 large-eddy turnover times.

magnetic spectrum in Run 256- $B_{\max}0.01$ -f3, which corresponds to the dashed curves in the left panel<sup>4</sup>. When  $t \lesssim 7.5L/v_{t=0}$ , magnetic energy spectrum peaks near the dissipation-scale wavenumber, which implies stretching is most active there, and the magnetic spectrum moves upward without changing its shape much. This behavior of magnetic spectrum is very similar to that of a driven turbulence. However, there are also differences<sup>5</sup>. First, the dissipation scale in the decaying turbulence gradually increases as turbulence decays. In incompressible hydro-

dynamic turbulence, the dissipation scale is  $\sim (Lv/\nu)^{3/4}$  times smaller than  $L$ . Therefore, as  $v$  goes down, the dissipation scale goes up. The eddy turnover time at the dissipation scale increases as  $v$  decreases and the dissipation scale increases. Second, as the eddy turnover time at the stretching scale (i.e. at the dissipation scale in this case) changes, the growth rate of magnetic energy density deviates from an exponential one, which is clearly observed in the left panel of Figure 8. At  $t \sim 7.5L/v_{t=0}$ , the magnetic spectrum ‘touches’ the velocity spectrum at the dissipation scale.

After  $t \sim 7.5L/v_{t=0}$ , the evolution of magnetic spectrum is somewhat complicated. When we compare magnetic spectra at  $t=7.5$  (dashed curves) and 24 (long-dashed curve), we find that magnetic spectrum for large  $k$  values goes down and that for small  $k$  values goes up after  $t \sim 7.5L/v_{t=0}$ . The spectrum for large  $k$  values decreases as the velocity spectrum decreases due to decay of turbulence. On the other hand, the spectrum for small

<sup>4</sup> The time evolution of magnetic spectra in Run 256- $B_{\max}0.01$ -f0 is qualitatively similar. The reason we show spectra of Run 256- $B_{\max}0.01$ -f3 is that they evolve more quickly due to the additional forcing.

<sup>5</sup> Since magnetic field fills most of the computational box reasonably fast (see the left panel) and evolution of the system after magnetic field fills the box is very similar to that of a weak uniform seed field case, the discussion below should be also applicable to the case with a weak uniform seed field.

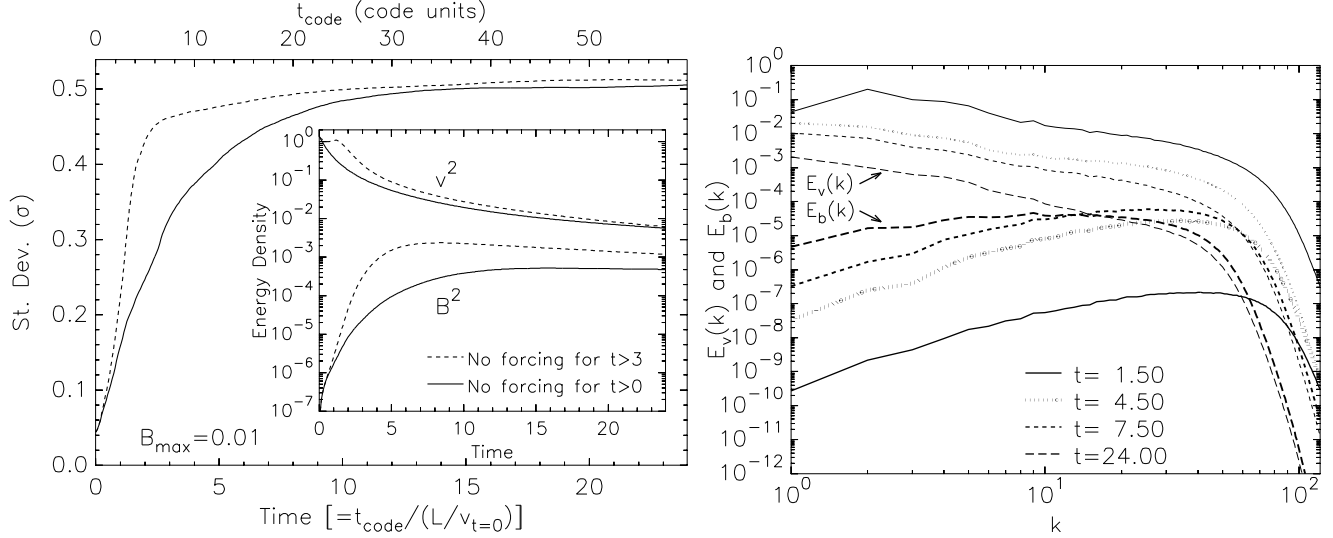


FIG. 8.— Purely decaying turbulence (Run 256- $B_{\text{max}}0.01\text{-f0}$ ; solid curves) and turbulence with short-lasting driving (Run 256- $B_{\text{max}}0.01\text{-f3}$ ; dashed curves). In the former, we let the turbulence decay at  $t=0$ . In the latter, we drive turbulence for  $t \leq 3$  and we stop driving after  $t = 3$ . (Left) Time evolution of energy densities (actually,  $B^2$  and  $v^2$ ) and the standard deviation of magnetic field distribution. Note that magnetic field spreads and amplifies even in purely decaying turbulence. (Right) Time evolution of energy spectra (from Run 256- $B_{\text{max}}0.01\text{-f3}$ ). Time is given in units of  $L/v_{t=0}$  ( $\sim 2.5$  in code units), where  $v_{t=0}$  ( $\sim 1$ ) is the velocity at  $t=0$ .

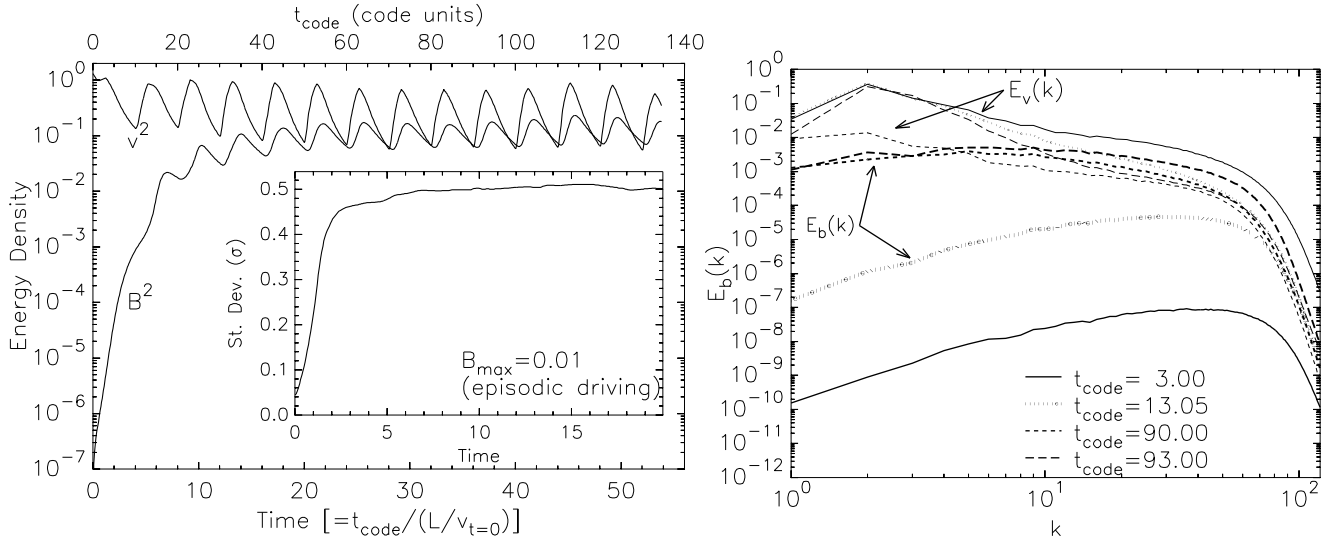


FIG. 9.— Turbulence with episodic forcing (Run 256- $B_{\text{max}}0.01\text{-f}_{\text{epi}}$ ). We repeat forcing (3 code time units) and no-forcing (7 code time units) every 10 code time units. (Left) Time evolution of energy densities (actually,  $B^2$  and  $v^2$ ) and the standard deviation of magnetic field distribution. We observe efficient growth and diffusion of magnetic field. (Right) Time evolution of energy spectra.

$k$  values increases because of stretching at large scales. As a result, the ratio  $B^2/v^2$  increases and the peak of the magnetic spectrum moves to larger scales. This behavior of  $E_b(k)$  will ultimately stop when the ratio  $B^2/v^2$  becomes large enough so that stretching at the outer scale of turbulence becomes suppressed. Note that, since magnetic spectrum for small  $k$  values increases and that for large  $k$  values decreases, the total magnetic energy density changes more slowly than the kinetic energy density (see the dashed curves for  $t \gtrsim 7.5$  in the left panel).

### 3.4. Turbulence with episodic driving

In order to have strong magnetization, we need either a continuous or a frequent episodic forcing. The left panel of Figure 9 shows that, if there are repeated mergers, we can have a relatively strong magnetic field. As in

other simulations, we have a fully developed turbulence and a localized seed magnetic field at  $t=0$ . In the simulation, we drive turbulence for 3 code time units and let it decay for 7 code time units. Then we repeat the same thing periodically. From the figure, it is evident that a ‘saturation stage’ is reached at  $t \sim 50$  in code units. After  $t \sim 50$  code time units,  $v^2$  and  $B^2$  do not show a systematic decrease or increase and just fluctuate around their average values. The inset shows that the standard deviation at  $t=10$  (in code units) is slightly smaller than the saturation value of 0.5. But the second episode of driving starting at  $t=10$  (in code units) quickly boosts it to the saturation value. The overall behavior of  $B^2$  and  $v^2$  is very similar to that in continuous-driving cases. Note that, during the decay stages after  $t \sim 50$  (in code units), magnetic energy density sometimes ex-



ceeds kinetic energy density, which is not observed in continuously driven turbulence (with  $\nu = \eta$ ). Therefore, it may be used to distinguish the driving mechanisms in the ICM.

The right panel of Figure 9 shows time evolution of energy spectra. During the growth stages (i.e.  $t \lesssim 50$  in code units), the overall behavior of magnetic spectrum is very similar to that in continuously driven cases. For example, during the rapid growth stage ( $t \lesssim 15$  in code units), magnetic spectrum peaks near the dissipation scale and moves upward without changing the shape much (see solid and dotted curves that represent  $E_b(k)$ ). This behavior of magnetic spectrum is very similar to that during the exponential growth stage in a continuously driven turbulence. The peak of magnetic spectrum moves to smaller wavenumbers during the slower growth stage ( $15 \lesssim t \lesssim 50$ ), which is similar to the behavior of magnetic spectrum during the ‘linear’ growth stage in a continuously driven turbulence. However, after  $t \gtrsim 50$ , magnetic and velocity spectra during the driving episodes are clearly different from those during the decay (i.e. no-forcing) phases. Let us compare spectra at  $t = 90$  (dashed curves) and 93 (long-dashed curves). Since an episode of driving starts at  $t = 90$  and ends in  $t = 93$  in code units, the dashed curves are spectra during the decay phase and the long-dashed curves are spectra at the end of the driving episode. Velocity spectrum during the decay phase (dashed curve) is clearly lower than that during the driving episode (long-dashed curve). Magnetic spectrum during the decay phase is also lower than that during the driving episode.

#### 4. DISCUSSION

In this paper, we have found that growth of a localized seed magnetic field is as fast as that of a uniform magnetic field. This result implies that magnetic field ejected from astrophysical bodies can be a viable origin of magnetic field in the large-scale structure of the universe.

Assuming a uniform seed magnetic field (and turbulence generated by cosmological shocks), Ryu et al. (2008) showed that turbulence in the ICM has almost reached the saturation stage. Our current simulations imply that we may arrive at a similar conclusion also in the case of a localized seed magnetic field. Therefore, we expect a strong magnetization in clusters regardless of the shape of the seed field, which makes the findings in Ryu et al. (2008) more reliable in clusters.

Since both a uniform and a localized seed fields give similar distributions and strengths of magnetic fields in clusters, it may be difficult to tell which seed field is more important. One may think that it would be more advantageous to look at magnetic field distributions in filaments. Indeed, we expect that large-eddy motions are slower in filaments and magnetic fields ejected from astrophysical bodies may not have enough time to fill the whole system (see also discussions in Brüggén et al 2005). Therefore, magnetic field distribution in filaments may be spatially inhomogeneous when seed magnetic fields are ejected from galaxies. Indeed, if  $t/(L/v) \lesssim 2$ , we expect to see spatially inhomogeneous distribution of magnetic fields in filaments (see Figures 5 and 6; see also the right panel of Figure 7). Even if  $t/(L/v)$  is larger, driving scale of turbulence can also affect spatial inhomogeneity.

If turbulence in filaments is driven on scales much smaller than the system size of a few Mpc, magnetic fields may not have enough time to diffuse over un-correlated eddies and, as a result, we may have spatially inhomogeneous magnetic field distributions.

On the other hand, if turbulence in a filament is driven by cosmological shocks, where driving scale of turbulence is comparable to the system size, we will have more or less homogeneous magnetic field distribution. Cho & Ryu (2009) argued that the driving scale of turbulence is comparable to the size of the system and that  $t/(L/v) \sim 4$  in a typical filament.<sup>6</sup> Figure 6 suggests that 4 large-eddy turnover times are more than enough to magnetize the whole outer-scale eddy and also adjacent outer-scale eddies, the total size of which is larger than a few Mpc. Therefore, unless the astrophysical sources that provide seed magnetic fields are very sparse, magnetic fields fill substantial volume fraction in filaments.

Our results show that magnetic diffusion is fast for  $B_{max} \leq 1$ . Note that, when  $B_{max} = 1$ , local magnetic energy density is comparable to kinetic energy density and magnetic backreaction is not negligible in the local region. Nevertheless, our simulations show overall magnetic diffusion by turbulence is not suppressed by the backreaction. In this paper, we do not consider stronger initial seed magnetic fields because we can guess what will happen. In case of  $B_{max} > 1$ , we expect that magnetic pressure first makes magnetic field spread outward, which should be faster than turbulence diffusion (see Colbert et al. 1996; Xu et al. 2010, 2011). Then, after local magnetic energy density drops below the kinetic energy density, turbulence becomes the major agent that makes magnetic field spread out, which we know from our current simulations is fast. Therefore we expect fast diffusion of the seed magnetic field even cases of  $B_{max} > 1$ .

We do not assume any specific origin of turbulence in this paper: unless the driving scale is much smaller than the system size, it does not matter much. Consider a cluster of galaxies. If turbulence is initiated by cosmological shocks (Ryu et al. 2003; Pfrommer 2006) or mergers (De Young 1992; Tribble 1993; Norman & Bryan 1999; Roettiger, Burns, & Stone 1999; Ricker & Sarazin 2001), we expect that the outer scale of turbulence is comparable to the size of the whole system. In fact, the outer scale of turbulence observed in some simulations during the formation of galaxy clusters is up to  $\sim$  several 100 kpc (Norman & Bryan 1999; Ricker & Sarazin 2001), which is a few times smaller than the cluster size of  $\sim$  Mpc. In our current simulations, the driving scale is about 2.5 times smaller than the simulation box. Therefore, our current simulations mimic turbulence generated by cosmological shocks or mergers. However, it is still possible that turbulence in the ICM is driven by infall of small structures (Takizawa 2005), AGN jets (see, for example, Scannapieco & Brüggén 2008), or galaxy wakes (Roland 1981; Bregman & David 1989; Kim 2007). In this case, the driving scale of turbulence can be much smaller than the size of the whole system. If we consider a

<sup>6</sup> Cho & Ryu (2009) used a different definition of the large-eddy turnover time. The large-eddy turnover time  $t_{eddy}$  in Cho & Ryu (2009) is roughly 2.5-3 times smaller than our large-eddy turnover time. Cho & Ryu (2009) found that  $t/t_{eddy} \sim 10$  for a typical filament, which is equivalent to  $\sim 4$  large-eddy turnover times in our definition here.

localized seed magnetic field inside an energy-containing eddy, we know that the seed field can spread and fill the outer-scale eddy fast. If the driving scale of turbulence is small, the subsequent stage of magnetic field diffusion may take a long time to fill the whole system because diffusion of magnetic field over un-correlated eddies may be slower compared with that inside an energy-containing eddy. We will address this issue elsewhere (Cho 2012, in preparation).

In this paper, we have considered homogeneous turbulence. However, turbulence in the ICM is not homogeneous. The ICM density varies from the core region to the cluster outskirts. Then how can it affect our results? The value of the ICM density length-scale may be an important factor<sup>7</sup>. If the length-scale is larger than the outer scale of turbulence, our results in this paper will not be affected much. On the other hand, if the opposite case is true, then it depends on the driving mechanism in the following way. First, if turbulence is initiated by a violent event/events and if the outer scale of turbulence does not change for a couple of large-eddy turnover times, then our results may not be affected much. If the outer scale of turbulence does not change, a couple of large-eddy turnover times would be enough for magnetic field to fill the most of the ICM. Second, if turbulence is initiated less violently, then it may be possible that the effective outer scale of turbulence reduces to a value comparable to the density length-scale. In this case, effective reduction of the outer scale can make the resulting turbulence similar to that with small-scale driving. Further numerical study will be necessary to test this possibility.

## 5. SUMMARY

In this paper, we have assumed that driving scale of turbulence is comparable to the size of the system, which can be justified if we consider ICM turbulence driven by mergers or cosmological shocks. We have found the following results:

1. The growth of a localized seed magnetic field is as

fast as that of a uniform seed magnetic field.

2. Turbulence diffusion of magnetic field is fast. When we insert a localized seed magnetic field in a turbulent medium, turbulent motions make it disperse and fill the whole system very fast, within  $\sim 3$  large-eddy turnover times. After magnetic field fills the whole system, the time evolution should be very similar to the case of a uniform seed magnetic field. This way, we have a fast growth of the seed magnetic field. Our result implies that even in filaments the volume filling factor of magnetic fields is of order unity if turbulence is driven on scales comparable to the size of the systems.
3. Growth and turbulence diffusion of a localized seed magnetic field in a high Prandtl number turbulence is also fast.
4. A localized seed magnetic field can ultimately fill the whole system even in a decaying turbulence. Therefore, we may have a wide-spread magnetic field in a cluster that has undergone just one major merger. Magnetic field can be injected at any time during the merger: our decaying turbulence simulation suggests that magnetic field can be injected even at the end of the merger. Although the strength of the resulting magnetic field is very weak in decaying turbulence, the wide-spread magnetic field can be used as a seed field in the next episode of merger.
5. Growth of a localized seed magnetic field in case of episodic driving is also fast.

This research was supported by National R & D Program through the National Research Foundation of Korea (NRF) funded by the Ministry of Education, Science and Technology (No. 2011-0018751). We thank the anonymous referee for constructive comments.

## REFERENCES

- Arieli, Y., Rephaeli, Y. & Norman, M. L. 2011, *ApJ*, 738, 15  
 Banerjee, R., & Jedamzik, K. 2003, *Phys. Rev. Lett.*, 91, 251301  
 Batchelor, G. 1950, *Proc. R. Soc. London A*, 201, 405  
 Bertone, S., Vogt, C., & Enßlin, T. 2006, *MNRAS*, 370, 319  
 Brandenburg, A. & Subramanian, K. 2005, *Phys. Reports*, 417, 1  
 Bregman, J. N., & David, L. P. 1989, *ApJ*, 341, 49  
 Brügggen, M., Ruszkowski, M., Simionescu, A., Hoeft, M., & Dalla Vecchia, C. 2005, *ApJ*, 631, L21  
 Childress, S., & Gilbert, A. 1995, *Stretch, Twist, Fold: The Fast Dynamo* (Berlin: Springer)  
 Cho, J., Lazarian, A., Honein, A., et al. 2003, *ApJ*, 589, L77  
 Cho, J., & Vishniac, E. T. 2000, *ApJ*, 538, 217  
 Cho, J., Vishniac, E. T., Beresnyak, A., Lazarian, A., & Ryu, D. 2009, *ApJ*, 693, 1449  
 Cho, J. & Ryu, D. 2009, *ApJL*, 705, 90  
 Colbert, E. J. M., Baum, S. A., Gallimore, J. F., O’Dea, C. P., & Christensen, J. A. 1996, *ApJ*, 467, 551  
 De Young, D. 1992, *ApJ*, 386, 464  
 Dolag, K., Bartelmann, M., & Lesch, H. 1999, *A&A*, 348, 351  
 Dolag, K., Bartelmann, M., & Lesch, H. 2002, *A&A*, 387, 383
- <sup>7</sup> In addition, magnetic buoyancy can also be an important factor. If a localized seed magnetic field is injected into the central region of the ICM, magnetic buoyancy will enhance the rate of magnetic diffusion.
- Donnert, J., Dolag, K., Lesch, H., Müller, E. 2009, *MNRAS*, 392, 1008  
 Dubois, Y., & Teyssier, R. 2008, *A&A*, 482, L13  
 Ensslin, T. A., Biermann, P. L., Kronberg, P. P., & Wu X. 1997, *ApJ*, 477, 560  
 Gnedin, N. Y., Ferrara, A., & Zweibel, E. G. 2000, *ApJ*, 539, 505  
 Kazantsev, A. P. 1968, *Soviet Phys.-JETP Lett.*, 26, 1031  
 Kim, W.-T. 2007, *ApJL*, 667, 5  
 Kronberg, P. P., 1994, *Rep. Prog. Phys.*, 57, 325  
 Kronberg, P. P., Lesch, H., & Hopp, U. 1999, *ApJ*, 511, 56  
 Kulsrud, R. & Anderson, S. 1992, *ApJ*, 396, 606  
 Kulsrud, R. M., Cen, R., Ostriker, J. P., & Ryu, D. 1997, *ApJ*, 480, 481  
 Kulsrud, R. M., & Zweibel, E. G. 2008, *Reports on Progress in Physics*, 71, 046901  
 Lesieur, M. 1990, in *Turbulence in Fluids: Stochastic and Numerical Modelling* (2d rev. ed.; Dordrecht: Kluwer), chap. 8  
 Murgia, M., Govoni, F., Feretti, L., Giovannini, G., Dallacasa, D., Fanti, R., Taylor, G. B., & Dolag, K. 2004, *A&A*, 424, 429  
 Norman, M. L., & Bryan, G. L. 1999, *Lecture Notes in Physics* Vol. 530: *The Radio Galaxy* Messier 87, 530, 106  
 Pfrommer, C., Springel, V., Enßlin, T. A., & Jubelgas, M. 2006, *MNRAS*, 367, 113  
 Rees, M. 1987, *QJRAS*, 28, 197  
 Rephaeli, Y. 1988, *Comments on Astrophysics*, 12, 265

TABLE 1  
SIMULATIONS.

Run	Resolution	$B_{max}$ at $t=0^a$	$B_0^b$	Pr,m <sup>c</sup>	forcing
256- $B_{max}0.001$	256 <sup>3</sup>	0.001	0.	1	continuous
256- $B_{max}0.01$	256 <sup>3</sup>	0.01	0.	1	continuous
256- $B_{max}0.1$	256 <sup>3</sup>	0.1	0.	1	continuous
256- $B_{max}1$	256 <sup>3</sup>	1	0.	1	continuous
512- $B_{max}0.01$	512 <sup>3</sup>	0.01	0.	1	continuous
256- $B_{max}0.01$ -Pr	256 <sup>3</sup>	0.01	0.	high	continuous
256- $B_{max}1$ -Pr	256 <sup>3</sup>	1	0.	high	continuous
512- $B_{max}0.01$ -Pr	512 <sup>3</sup>	0.01	0.	high	continuous
256- $B_{max}0.01$ -f0	256 <sup>3</sup>	0.01	0	1	no forcing
256- $B_{max}0.01$ -f3	256 <sup>3</sup>	0.01	0	1	$t \leq 3$ in code units
256- $B_{max}0.01$ -f $_{epi}$	256 <sup>3</sup>	0.01	0	1	episodic
REF256	256 <sup>3</sup>	-	10 <sup>-4</sup>	1	continuous
REF256-Pr	256 <sup>3</sup>	-	10 <sup>-4</sup>	high	continuous

<sup>a</sup> Maximum value of the random field at  $t=0$ .<sup>b</sup> Strength of the mean field.<sup>c</sup> Magnetic Prandtl number ( $\equiv \nu/\eta$ ).

Reynolds, C. S., McKernan, B., Fabian, A. C., Stone, J. M., & Vernaleo, J. C. 2005, MNRAS, 357, 242  
Ricker, P. M., & Sarazin, C. L. 2001, ApJ, 561, 621  
Roettiger, K., Stone, J. M., & Burns, J. O., 1999a, ApJ, 518, 594  
Roland, J. 1981, A&A, 93, 407  
Ruszkowski, M., Brügggen, M., & Begelman, M. C. 2004, ApJ, 611, 158  
Ryu, D., Kang, H., Cho, J., & Das, S. 2008, Science, 320, 909  
Ryu, D., Kang, H., Hallman, E., & Jones, T. W. 2003, ApJ, 593, 599  
Scannapieco, E., & Brügggen, M. 2008, ApJ, 686, 927  
Schekochihin, A. A., Cowley, S. C., Taylor, S. F., Maron, J. L., & McWilliams, J. C. 2004, ApJ, 612, 276

Schekochihin, A. & Cowley, S. 2007, in *Magnetohydrodynamics - Historical evolution and trends*, eds. by S. Molokov, R. Moreau, & H. Moffatt (Berlin; Springer), p. 85. (astro-ph/0507686)  
Subramanian, K., Shukurov, A. & Haugen, N. 2006, MNRAS, 366, 1437  
Spitzer, L. 1962, *Physics of Fully Ionized Gases* (New York: Wiley)  
Takizawa, M. 2005, ApJ, 629, 791  
Tribble, P. C. 1993, MNRAS, 263, 31  
Völk, H. J., & Atoyan A. M. 2000, ApJ, 541, 88  
Xu, H., Li, H., Collins, D. C., Li, S., & Norman, M. L. 2010, ApJ, 725, 2152  
Xu, H., Li, H., Collins, D. C., Li, S., & Norman, M. L. 2011, ApJ, 739, 77  
Zeldovich, Ya. B., Ruzmaikin, A. A., Molchanov, S. A., & Sokoloff, D. D. 1984, J. Fluid Mech., 144, 1